

Numerical Solution of Heat Transfer in MHD Mixed Convection Flow Micropolar Casson Fluid about Solid Sphere with Radiation Effect

Husein A. Alzgool¹, Hamzeh T. Alkawasbeh^{2*}, Sana Abu-ghurra², Zain Al-hour³, Mohammed Z. Swalmeh⁴

¹Department of Civil Engineering, Faculty of Engineering, Ajloun National University, P.O. Box 43, Ajloun 26810, Jordan.

²Department of Mathematics, Faculty of Science, Ajloun National University, P.O. Box 43, Ajloun 26810, Jordan.

³Department of Civil Engineering, Faculty of Engineering, Ajloun National University, P.O. Box 43, Ajloun 26810, Jordan.

⁴Faculty of Informatics and Computing, Universiti Sultan Zainal Abidin (Kampus Gong Badak), 21300 Kuala Terengganu, Terengganu, Malaysia.

*Corresponding Author

Abstract

This study is conducted to develop a numerical solution of heat transfer in magneto-hydrodynamic mixed convection flow micropolar Casson fluid about solid sphere. The radiation effects are also considered in the energy equation. The governing momentum energy and angular momentum equations are transformed into nonlinear partial differential equations by the use of a non-similarity transformation. These equations are solved numerically subject to an appropriate physical boundary conditions using an implicit finite difference scheme known as the Keller-box method. Several parameters namely the mixed convection parameter λ , Casson fluid parameter β , magnetic parameter M , radiation parameter R and micropolar parameter K have been involved in the problem. The effect of these parameters on the local Nusselt number and on the local skin friction coefficient, as well as on the temperature, velocity and angular velocity profiles are illustrated graphically. The obtained results are validated with previously published available results and are found to be in good agreement.

Keywords: Magneto-hydrodynamic (MHD), Mixed Convection, Heat Transfer, Micropolar Casson Fluid, Solid Sphere, Radiation

INTRODUCTION

Casson fluids in the presence of heat transfer is widely used in the processing of chocolate, foams, syrups, nail, toffee and many other foodstuffs Ramachandra et al [1]. Casson [2], in his pioneering work introduced this model to simulate industrial inks. Later on, a substantial research has been done on the Casson fluid flow because of its important engineering applications. Mustafa et al [3] have studied the heat transfer flow of a Casson fluid over an impulsive motion of the plate using the homotopy method. The exact solution of forced convection boundary layer Casson fluid flow toward a linearly stretching surface with transpiration effects are reported by Mukhopadhyay et al [4]. In the same year, Subba et al [5] considered the velocity and thermal slip conditions on the laminar boundary layer heat transfer flow of a Casson fluid past a vertical plate. Mahdy and Ahmed [6] studied the effect

of magneto-hydrodynamic on a mixed convection boundary flow of an incompressible Casson fluid in the stagnation point of an impulsively rotating sphere. The convective boundary layer flow of Casson nanofluid from an isothermal sphere surface is presented by Nagendra et al [7]. Mehmood et al [8] investigated the micropolar Casson fluid on mixed convection flow induced by a stretching sheet. Shehzad et al [9] discussed the viscous chemical reaction effects on the MHD flow of a Casson fluid over a porous stretching sheet. Recently, Khalid et al [10] developed exact solutions for unsteady MHD free convection flow of a Casson fluid past an oscillating plate.

Included in the class of several other non-Newtonian fluid models namely the micropolar fluids are fluids belong to a class of fluids with non-symmetric stress tensor, they are fluids with microstructure. Micropolar fluids may represent fluids consisting of rigid, spherical oriented particles suspended in the viscous medium, where disfigurement of fluid particles is ignored. The model of micropolar fluids were firstly introduced by Eringen [11]. Further, many physicists, engineers and mathematicians studied the micropolar fluid to conclude different results related to flow problems. Hassanien et al [12] presented the boundary layer flow and heat transfer from a stretching sheet to a micropolar fluid. Papautsky et al [13] investigated the laminar fluid behavior in microchannel using micropolar fluid theory. Nazar et al [14] Considered stagnation point flow of a micropolar fluid towards a stretching sheet. Exact solutions are obtained using the Laplace transform technique for the unsteady flow of a micropolar fluid Sherief et al [15]. Hussanan et al [16] studied the effects of various physical parameters on velocity and microrotation. Hussanan et al [17] explained the unsteady natural convection flow of a micropolar fluid on a vertical plate oscillating in its plane with Newtonian heating condition. The free convection boundary layer flow of micropolar fluid on a solid sphere with convective boundary conditions was considered by Alkawasbeh et al [18]. Alkawasbeh [19] explored the heat transfer magneto-hydrodynamic flow of micropolar Casson fluid on a horizontal circular cylinder with thermal radiation. The natural convection on boundary layer flow of Cu-water and Al₂O₃-water micropolar nanofluid about a solid sphere investigated by Swalmeh et al [20]. Micropolar forced convection flow over moving surface under magnetic field was inspected by Waqas et al [21].

The heat transfer through a boundary layer in the mixed convection flow about a sphere has a vast space in applied technology, such as solving the cooling problems in turbine blades, electronic systems and manufacturing processes, experiments on heat transfer between spheres and airflow Yuge [22]. Recently, the various papers in mixed convection boundary-layer flow for an isothermal solid sphere with different types of fluids was presented by Hieber and Gebhart [23], Chen and Mucoglu [24], Dennis and Walker [25], Tham et al [26] and Alkasasbeh et al [27].

The objective of this paper is to study the MHD mixed convection boundary layer flow over a solid sphere in a micropolar Casson fluid with thermal radiation. The boundary-layer equations are solved numerically via efficient implicit finite-difference scheme known as the Keller-box method, as displayed by Cebeci and Bradshaw [28]. For comparison purposes, the present results for $Pr = 7, M = R = K = 0$ and $\beta \rightarrow \infty$, (regular Newtonian fluid) are computed.

MATHEMATICAL MODELING

Consider the impermeable solid sphere of radius a , which is placed in an incoming stream of micropolar Casson fluid with an undisturbed free-stream velocity U_∞ and constant temperature T_∞ , with steady mixed convection boundary-layer flow. The convective forced flow is assumed to be moving upward, while the gravity vector g acts downward in the opposite direction as displayed in Figure 1, where \bar{x} -coordinate is measured along the circumference of the solid sphere from the lower stagnation point, \bar{y} -coordinate is measured normal to the surface of the sphere. It is also assumed that the surface of the sphere is maintained at a constant temperature, T_w with $T_w > T_\infty$ for a heated sphere (assisting flow) and $T_w < T_\infty$ for a cooled sphere (opposing flow).

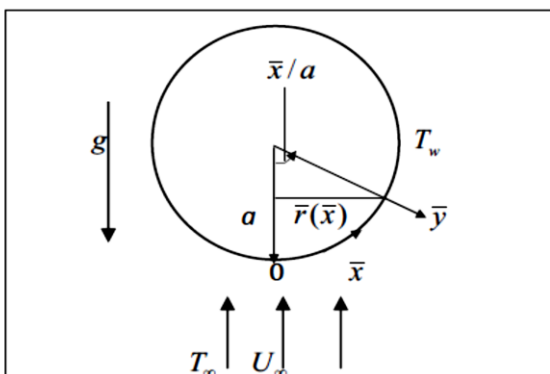


Fig. 1: Physical model and coordinate system for the mixed convection

The constitutive relationship for an incompressible Casson fluid flow as reported by Mukhopadhyay et al [4]:

$$\tau_{ij} = \begin{cases} 2(\mu_B + p_y \sqrt{2\pi}) e_{ij} & \pi > \pi_c, \\ 2(\mu_B + p_y \sqrt{2\pi_c}) e_{ij} & \pi < \pi_c, \end{cases}$$

where $\pi = e_{ij} e_{ij}$, e_{ij} is the (i, j) -th component of the deformation rate, μ_B is the plastic dynamic viscosity of the non-Newtonian fluid, π_c is a critical value of this product based on the non-Newtonian model and p_y is the yield stress of the fluid.

Introducing the boundary layer approximations, the continuity, momentum, microrotation and energy equations, can be written as follows, respectively:

$$\frac{\partial}{\partial \bar{x}} (\bar{r} \bar{u}) + \frac{\partial}{\partial \bar{y}} (\bar{r} \bar{v}) = 0, \quad (1)$$

$$\begin{aligned} \bar{u} \frac{\partial \bar{u}}{\partial \bar{x}} + \bar{v} \frac{\partial \bar{u}}{\partial \bar{y}} = \bar{u}_e \frac{d\bar{u}_e}{d\bar{x}} + \left(\frac{\mu + \kappa}{\rho} \right) \left(1 + \frac{1}{\beta} \right) \frac{\partial^2 \bar{u}}{\partial \bar{y}^2} \\ + gB(T - T_\infty) \sin\left(\frac{\bar{x}}{a}\right) + \frac{\kappa}{\rho} \frac{\partial \bar{H}}{\partial \bar{y}} - \frac{\sigma B_0^2}{\rho} \bar{u} \end{aligned} \quad (2)$$

$$\rho j \left(\bar{u} \frac{\partial \bar{H}}{\partial \bar{x}} + \bar{v} \frac{\partial \bar{H}}{\partial \bar{y}} \right) = -\kappa \left(2\bar{H} + \frac{\partial \bar{u}}{\partial \bar{y}} \right) + \phi \frac{\partial^2 \bar{H}}{\partial \bar{y}^2}, \quad (3)$$

$$\bar{u} \frac{\partial T}{\partial \bar{x}} + \bar{v} \frac{\partial T}{\partial \bar{y}} = \alpha \frac{\partial^2 T}{\partial \bar{y}^2} - \frac{1}{\rho c_p} \frac{\partial q_r}{\partial \bar{y}} \quad (4)$$

These equations are subjected to the boundary conditions Nazar et al [29],

$$\bar{u} = \bar{v} = 0, T = T_w, \bar{H} = -\frac{1}{2} \frac{\partial \bar{u}}{\partial \bar{y}} \text{ as } \bar{y} = 0,$$

$$\bar{u} \rightarrow \bar{u}_e(\bar{x}), T \rightarrow T_\infty, H \rightarrow 0, \text{ as } \bar{y} \rightarrow \infty, \quad (5)$$

where \bar{u} and \bar{v} are the velocity components along the \bar{x} and \bar{y} directions, respectively. \bar{H} is the angular velocity of micropolar fluid, κ is the vortex viscosity, T is the local temperature, g is the gravity acceleration, k is the thermal conductivity, σ is the electric conductivity, α is the thermal diffusivity, B is the thermal expansion coefficient, β_0^2 is the magnetic field strength, ν is the kinematic viscosity, μ is the dynamic viscosity, ρ is the fluid density, c_p is the specific heat, $j = a^2 / \sqrt{Gr}$ is the microinertia density, $\beta = \mu_B \sqrt{2\pi_c} / p_y$ is the parameter of the Casson fluid and the spin gradient viscosity $\phi = (\mu + \kappa / 2) j$, the radial distance from the

symmetrical axis to the surface of the sphere $\bar{r}(\bar{x}) = a \sin(\bar{x}/a)$, and the free stream velocity $\bar{u}_e(\bar{x}) = U_\infty \sin(\bar{x}/a)$

We introduce now the following non-dimensional variables Nazar et al [29],

$$x = \frac{\bar{x}}{a}, \quad y = \text{Re}^{1/2} \left(\frac{\bar{y}}{a} \right), \quad r(x) = \frac{\bar{r}(\bar{x})}{a},$$

$$u = \frac{\bar{u}}{U_\infty}, \quad v = \text{Re}^{1/2} \left(\frac{\bar{v}}{U_\infty} \right), \quad H = \left(\frac{a}{U_\infty} \right) \text{Re}^{-1/2} \bar{H}, \quad \theta = \frac{T - T_\infty}{T_w - T_\infty}, \quad (6)$$

where $\text{Re} = U_\infty(a/\nu)$ is the Reynolds number. Using the Rosseland approximation for radiation, the radiative heat flux is simplified as (Bataller [30])

$$q_r = -\frac{4\sigma^*}{3k^*} \frac{\partial T^4}{\partial y}, \quad (7)$$

where σ^* and k^* are the Stefan-Boltzmann constant and the mean absorption coefficient, respectively. We assume that the temperature differences within the flow through the micropolar fluid such as that the term T^4 may be expressed as a linear function of temperature. Hence, expanding T^4 in a Taylor series about T_∞ and neglecting higher-order terms, we get

$$T^4 \cong 4T_\infty^3 T - 3T_\infty^4. \quad (8)$$

Substituting variables (6)–(8) into equations (1)–(4), we obtain the following non-dimensional equations of the problem under consideration:

$$\frac{\partial}{\partial x}(ru) + \frac{\partial}{\partial y}(rv) = 0, \quad (8)$$

$$u \frac{\partial u}{\partial x} + v \frac{\partial u}{\partial y} = u_e \frac{du_e}{dx} + \left(1 + K + \frac{1}{\beta} \right) \frac{\partial^2 u}{\partial y^2} + \lambda \theta \sin x + -Mu + K \frac{\partial H}{\partial y} \quad (9)$$

$$u \frac{\partial H}{\partial x} + v \frac{\partial H}{\partial y} = -K \left(2H + \frac{\partial u}{\partial y} \right) + \left(1 + \frac{K}{2} \right) \frac{\partial^2 H}{\partial y^2}, \quad (10)$$

$$u \frac{\partial \theta}{\partial x} + v \frac{\partial \theta}{\partial y} = \frac{1}{\text{Pr}} \left(1 + \frac{4}{3} R \right) \frac{\partial^2 \theta}{\partial y^2}, \quad (11)$$

The boundary conditions (5) become

$$u = v = 0, \quad \theta = 1, \quad H = -\frac{1}{2} \frac{\partial u}{\partial y} \text{ at } y = 0,$$

$$u_e(x) \rightarrow \frac{3}{2} \sin x, \quad \theta \rightarrow 0, \quad H \rightarrow 0 \text{ as } y \rightarrow \infty. \quad (12)$$

Where $K = \kappa/\mu$ is the material or micropolar parameter, $\text{Pr} = \nu/\alpha$ is the Prandtl number, $M = \sigma B^2 a / \rho U_\infty$ is the

magnetic parameter and $R = \alpha k^* \rho c_p / 4\sigma^* T_\infty^3$ is the radiation and λ is the mixed convection parameter which is given by:

$$\lambda = \frac{Gr}{\text{Re}^2}, \quad (13)$$

with $Gr = gB(T_w - T_\infty)a^3/\nu^2$ is the Grashof number. Also, it is worth mentioning that $\lambda > 0$ corresponds to the assisting flow (heated sphere), $\lambda < 0$ corresponds to the opposing flow (cooled sphere) and $\lambda = 0$ corresponds to the forced convection flow.

To solve the system of equations (8) to (11) subjected to the boundary conditions (12), we assume the following variables:

$$\psi = xr(x)f(x, y), \quad \theta = \theta(x, y), \quad H = xh(x, y), \quad (14)$$

where ψ is the stream function defined as

$$u = \frac{1}{r} \frac{\partial \psi}{\partial y} \quad \text{and} \quad v = -\frac{1}{r} \frac{\partial \psi}{\partial x}, \quad (15)$$

which satisfies the continuity equation (8). Thus, equations (9) to (11) become

$$\left(1 + K + \frac{1}{\beta} \right) \frac{\partial^3 f}{\partial y^3} + (1 + x \cot x) f \frac{\partial^2 f}{\partial y^2} - \left(\frac{\partial f}{\partial y} \right)^2 + \lambda \frac{\sin x}{x} \theta - M \frac{\partial f}{\partial y} + \frac{9 \sin x \cos x}{4x} + K \frac{\partial h}{\partial y} = x \left(\frac{\partial f}{\partial y} \frac{\partial^2 f}{\partial x \partial y} - \frac{\partial f}{\partial x} \frac{\partial^2 f}{\partial y^2} \right) \quad (16)$$

$$\left(1 + \frac{K}{2} \right) \frac{\partial^2 h}{\partial y^2} + (1 + x \cot x) f \frac{\partial h}{\partial y} - \frac{\partial f}{\partial y} h - K \left(2h + \frac{\partial^2 f}{\partial y^2} \right) = x \left(\frac{\partial f}{\partial y} \frac{\partial h}{\partial x} - \frac{\partial f}{\partial x} \frac{\partial h}{\partial y} \right), \quad (17)$$

$$\frac{1}{\text{Pr}} \left(1 + \frac{4}{3} R \right) \frac{\partial^2 \theta}{\partial y^2} + f \frac{\partial \theta}{\partial y} = x \left(\frac{\partial f}{\partial y} \frac{\partial \theta}{\partial x} - \frac{\partial f}{\partial x} \frac{\partial \theta}{\partial y} \right), \quad (18)$$

Subject to the boundary conditions

$$f = \frac{\partial f}{\partial y} = 0, \quad \theta = 1, \quad h = -\frac{1}{2} \frac{\partial^2 f}{\partial y^2} \text{ at } y = 0,$$

$$\frac{\partial f}{\partial y} \rightarrow \frac{3 \sin x}{2x}, \quad \theta \rightarrow 0, \quad h \rightarrow 0 \text{ as } y \rightarrow \infty. \quad (19)$$

It can be seen that at the lower stagnation point of the sphere ($x \approx 0$), equations (16) and (18) reduce to the following ordinary differential equations:

$$\left(1 + K + \frac{1}{\beta}\right) f''' + 2ff'' - f'^2 + \lambda\theta - Mf' + Kh' + \frac{9}{4} = 0, \quad (20)$$

$$\left(1 + \frac{K}{2}\right) h'' + 2fh' - f'h - K(2h + f'') = 0, \quad (21)$$

$$\frac{1}{\text{Pr}} \left(1 + \frac{4}{3}R\right) \theta'' + f\theta' = 0. \quad (22)$$

and the boundary conditions (19) become

$$f(0) = f'(0) = 0, \theta(0) = 1, h(0) = -\frac{1}{2}f''(0),$$

$$f' \rightarrow \frac{3}{2}, \theta \rightarrow 0, h \rightarrow 0 \text{ as } y \rightarrow \infty, \quad (23)$$

Where primes denote differentiation with respect to y .

The physical quantities of interest in this problem are the local skin friction coefficient C_f and the local Nusselt number Nu which are defined by

$$C_f = \frac{a}{U_\infty} \text{Re}^{-1/2} \left(\mu + \frac{\kappa}{2} + \frac{P_y}{\sqrt{2\pi_c}} \right) \left(\frac{\partial \bar{u}}{\partial \bar{y}} \right)_{\bar{y}=0},$$

$$Nu = \frac{a}{k(T_f - T_\infty)} \text{Re}^{-1/2} \left(\frac{\partial \bar{T}}{\partial \bar{y}} \right)_{\bar{y}=0} \quad (24)$$

Using the non-dimensional variables (6)-(8) and the boundary conditions (13), the local skin friction coefficient C_f and the local Nusselt number Nu are:

$$C_f = \left(1 + \frac{K}{2} + \frac{1}{\beta}\right) x \left(\frac{\partial^2 f}{\partial y^2} \right)_{y=0},$$

$$Nu = - \left(1 + \frac{4}{3}R\right) \left(\frac{\partial \theta}{\partial y} \right)_{y=0}. \quad (25)$$

NUMERICAL SOLUTION

Equations (16) to (18) subject to boundary conditions (19) are solved numerically using the Keller-box method. This method seems to be the most flexible among the common methods and despite recent developments in other numerical methods, it remains a powerful and very accurate approach for parabolic boundary layer flows. It is also easily adaptable to solve equations of any order and unconditionally stable on the

solutions Cebeci and Bradshaw [28]. The following four steps have been used to obtain the solution

- i. Reduce the transformed equations (16) to (18) to a first-order system.
- ii. Write the difference equations using central differences.
- iii. Linearize the resulting algebraic equations by Newton's method and write them in matrix-vector form.
- iv. Use the block tridiagonal elimination technique to solve the linear system.

In numerical calculation, the suitable step size Δy and boundary layer thickness y_∞ must be determined. These suitable values must be defined so that the numerical results for the quantities discussed is not affected by Δy and y_∞ . Usually, we choose the step size $\Delta y = 0.2$ and we run the simulation until y_∞ . Moreover, the step size for the position x is chosen as $\Delta x = 0.005$ is sufficient to provide accurate numerical results.

RESULTS AND DISCUSSIONS

Equations (16)–(18) subject to the boundary conditions (19) have been solved numerically using an efficient implicit finite-difference scheme known as the Keller-box method, along with Newton's linearization technique as described by Cebeci and Bradshaw [28] for several values of parameters namely the Casson parameter β , the magnetic parameter M , the radiation parameter R , the mixed convection parameter λ , Prandtl number Pr , and the micro-rotation parameter K on the Nusselt number, skin friction coefficient, temperature, velocity and angular velocity fields, at some streamwise positions x for both the assisting ($\lambda > 0$) and opposing ($\lambda < 0$) flow cases. The solutions of nonlinear partial differential equations start at the lower stagnation point $x \approx 0$ up to $x = 120^\circ$ due to the probability of boundary layer separation occur after this point around the circumference of a solid sphere with initial profiles as given by the equations (19) to (21). Tables 1, presenta comparison between the results of this study and previously published results reported by Nazar et al [31] at $\text{Pr} = 7, M = R = K = 0$ and $\beta \rightarrow \infty$, (regular Newtonian fluid) for various values of λ . The comparison showed a good agreement indicating that the Keller-box method is suitable for solving this type of problem.

Figures 2 and 3 illustrate the influence of the Casson parameter on the local Nusselt number Nu and the local skin friction, respectively. It is seen from these figures that an increase of the Casson parameter leads to an increase in the local Nusselt number and decreases in the local skin friction. Moreover, as the value of x increases, the rate value of the local Nusselt number decreases and the local skin friction increases.

Table 1. Comparison of numerical values of local Nusselt number Nu at $Pr = 7, M = R = K = 0$ and $\beta \rightarrow \infty$, (Newtonian fluid), for various values of x and λ . Values in parenthesis are those of Nazar et al [31].

x	λ							
	-4	-3	-2	-1	-0.5	0.0	0.74	0.75
0°	0.6518 (0.6534)	0.7094 (0.7108)	0.7516 (0.7529)	0.7858 (0.7870)	0.8009 (0.8021)	0.8149 (0.8162)	0.8342 (0.8354)	0.8344 (0.8357)
10°	0.6430 (0.6440)	0.7030 (0.7040)	0.7461 (0.7470)	0.7808 (0.7818)	0.7961 (0.7970)	0.8106 (0.8112)	0.8300 (0.8307)	0.8300 (0.8309)
20°	0.6146 (0.6150)	0.6836 (0.6845)	0.7299 (0.7305)	0.7663 (0.7669)	0.7821 (0.7827)	0.7968 (0.7974)	0.8167 (0.8173)	0.8174 (0.8176)
30°		0.6499 (0.6507)	0.7026 (0.7027)	0.7421 (0.7422)	0.7589 (0.7591)	0.7743 (0.7746)	0.7952 (0.7955)	0.7955 (0.7958)
40°		0.5970 (0.5977)	0.6632 (0.6628)	0.7079 (0.7076)	0.7264 (0.7261)	0.7431 (0.7429)	0.7654 (0.7652)	0.7656 (0.7655)
50°			0.6093 (0.6080)	0.6633 (0.6624)	0.6843 (0.6836)	0.7029 (0.7022)	0.7272 (0.7267)	0.7276 (0.7270)
60°			0.5333 (0.5309)	0.6069 (0.6055)	0.6321 (0.6309)	0.6536 (0.6525)	0.6810 (0.6800)	0.6827 (0.6803)
70°				0.5470 (0.5224)	0.5686 (0.5668)	0.5949 (0.5934)	0.6267 (0.6253)	0.6287 (0.6257)
80°				0.4377 (0.4342)	0.4904 (0.4879)	0.5257 (0.5236)	0.5645 (0.5672)	0.5668 (0.5632)
90°					0.3835 (0.3796)	0.4425 (0.4398)	0.4941 (0.4920)	0.4968 (0.4926)
100°						0.3345 (0.3263)	0.4144 (0.4120)	0.4175 (0.4127)
110°							0.3206 (0.3179)	0.3248 (0.3192)
120°								0.1688 (0.1276)

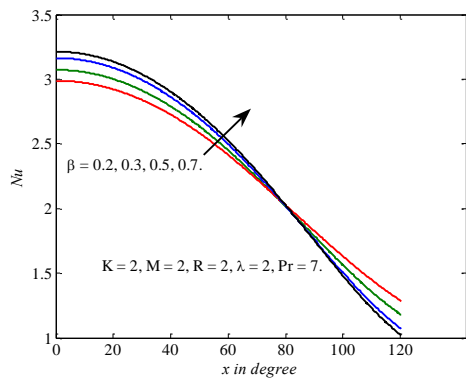


Fig. 2: Effect of the local Nusselt number for various values of the Casson parameter

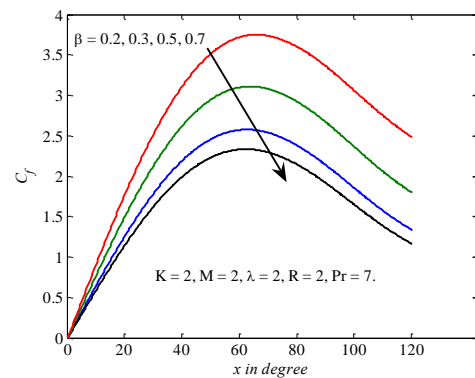


Fig. 3: Effect of the local skin friction for various values of the Casson parameter

Figures 4 and 5 depict the influence of the radiation parameter R , on the local Nusselt number and local skin friction, respectively. An increase in R from 0 (non-Radiation case) to 3, strongly accelerates the flow, i.e., increasing in a local skin friction coefficient and local Nusselt number values. In all profiles, a peak arises near the surface of the sphere and this peak is displaced progressively closer to the wall with an increase in R values.

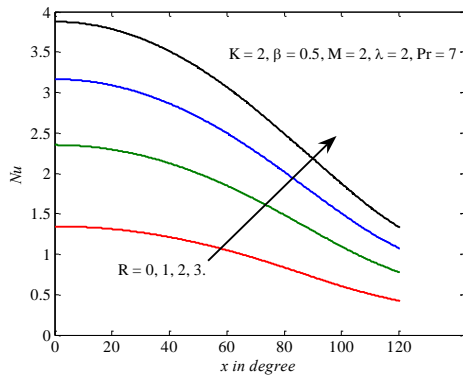


Fig. 4: Effect of the local Nusselt number for various values of the radiation parameter

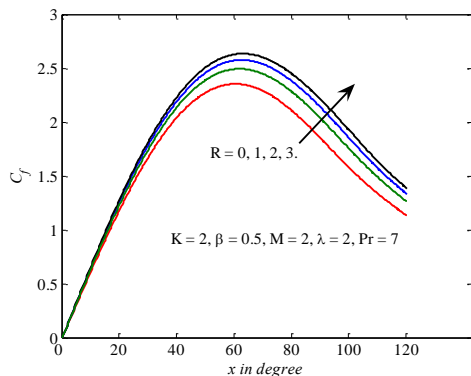


Fig. 5: Effect of the local skin friction for various values of the radiation parameter

Figures 6 and 7 represent the variation of local Nusselt number Nu and local skin friction coefficient C_f with different values of mixed convection parameter λ . From these figures, it is found that the increase of λ results in increase of Nu and C_f . Across the sphere surface, Nu and C_f increase before turning into decreasing approach.

Figures 8-9 illustrate the effect of the micro-rotation parameter K on the local Nusselt number and the local skin friction, respectively. It is seen from these figures that an increase of the micro-rotation parameter leads to decrease in the local Nusselt number and increase in the local skin friction.

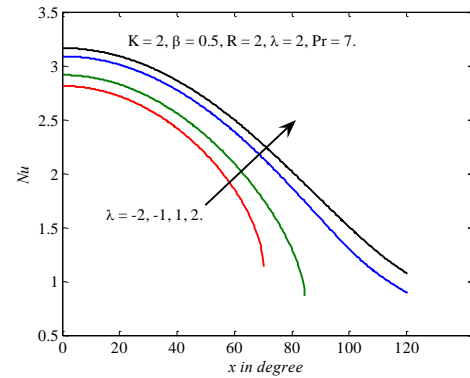


Fig. 6 Effect of the local Nusselt number for various values of the mixed convection parameter

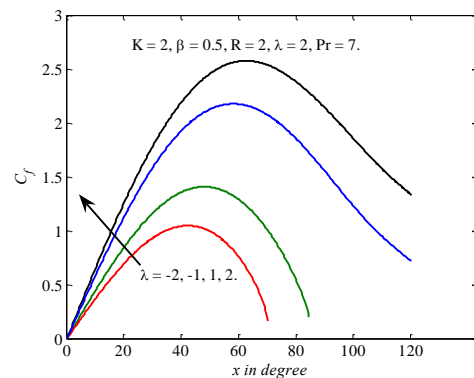


Fig. 7 Effect of the local skin friction for various values of the mixed convection parameter

The behaviour of magnetic parameter M on the local Nusselt number Nu and local skin friction C_f is illustrated in Figures 10-11. It is observed that the local Nusselt number and the local skin friction increased with the decrease in M . This behaviour is in accordance with the physical observation that the application of transverse magnetic field always results in a resistive type force also called Lorentz force. This type of resisting force tends to resist the fluid flow and thus reducing the fluid motion significantly.

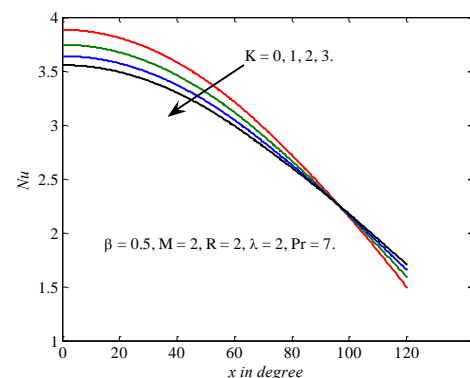


Fig. 8: Effect of the local Nusselt number for various values of the micro-rotation parameter.

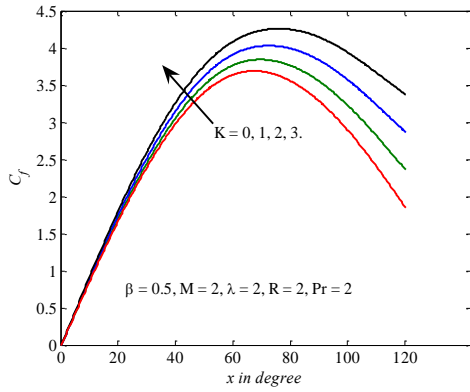


Fig. 9: Effect of the local Nusselt number for various values of the micro-rotation parameter.

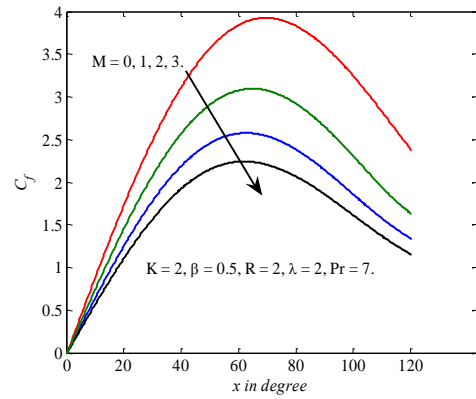


Fig. 11: Effect of the local skin friction for various values of the magnetic parameter

The influence of Casson parameter on temperature, velocity, and angular velocity profiles are exhibited in Figures 12-14. Figure 12 depicts that the temperature profiles $\theta(0, y)$ increase as the values of β decrease. While Figure 13 indicates that an increase in β tends to result in a decrease in the velocity profiles $(\partial f / \partial y)(0, y)$. This is true because as appeared in the shear term of the momentum equation (15), an increase in β implies a decrease in yield stress of the Casson fluid. Figure 13 shows that as Casson parameter β increases, the angular velocity profiles $h(0, y)$ also increase. Physically, an increase in Casson parameter means a decrease in yield stress and an increase in the plastic dynamic viscosity of the fluid which makes the momentum boundary layer thicker. This effectively slows down the fluid motion.

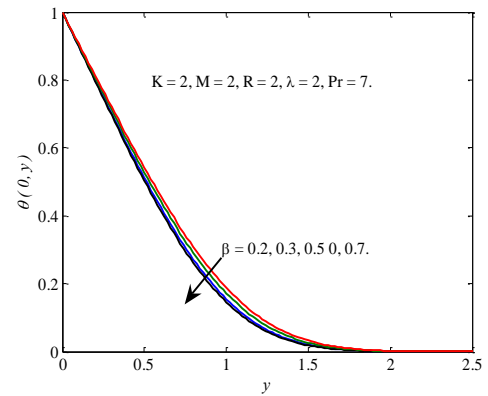


Fig. 12: Effect of the temperature profile for various values of the Casson parameter

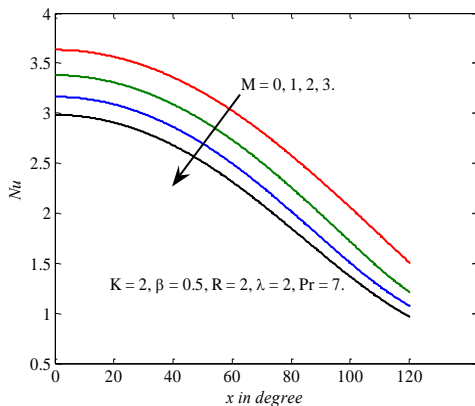


Fig. 10: Effect of the local Nusselt number for various values of the magnetic parameter

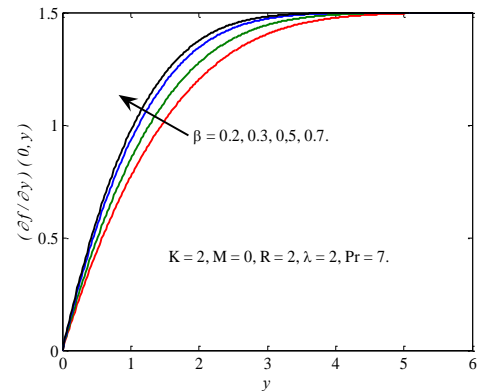


Fig. 13: Effect of velocity field for various values of the Casson parameter

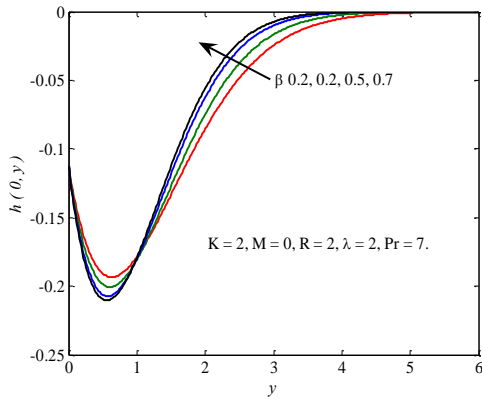


Fig. 14: Effect of the angular profile for various values of the Casson parameter

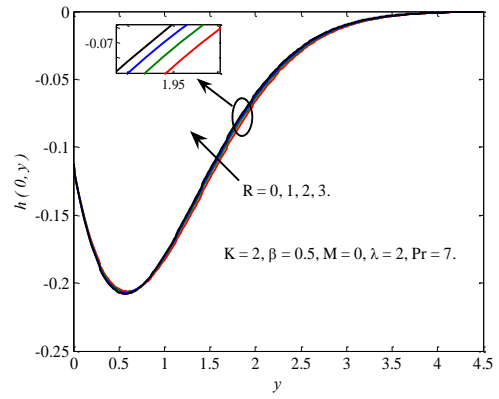


Fig. 17: Effect of angular velocity field for various values of the radiation parameter

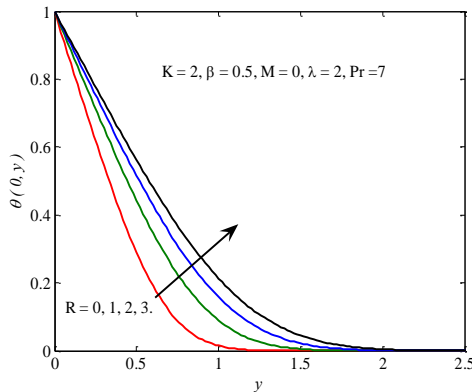


Fig. 15: Effect of the temperature profile for various values of the radiation parameter

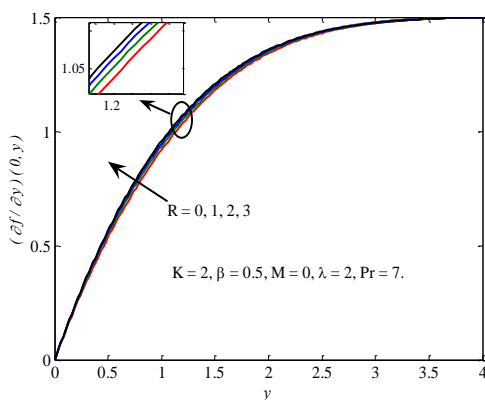


Fig. 16: Effect of velocity field for various values of the radiation parameter

Figures 15-17 present the effect of the radiation parameter R on temperature, velocity, and angular velocity profiles. The observation shows that the temperature, velocity, and angular velocity profiles increase with an increase in R because increasing the value of radiation parameter provides more heat to the fluid that causes an enhancement in the temperature, velocity, angular velocity profiles and the thickness of thermal boundary layer.

Figures 18-20 present the effect of the mixed convection parameter λ on the temperature, velocity, and angular velocity profiles. It should be noted that ($\lambda > 0$) corresponds to pure assisting flow (heated sphere) while ($\lambda < 0$) corresponds to opposing flow (cooled sphere). In these figures, it is predicted that the velocity and angular velocity increase while the temperature decreases as λ increases. This is due to the fact that when λ (i.e., buoyancy effects) increases, the convection cooling effect increases and hence the fluid flow accelerates.

Figures 21-23 display the temperature velocity and angular velocity profiles for different values of the micro-rotation parameter K . It is found as K increases the values of temperature profiles increase, but the velocity and angular velocity profiles decrease.

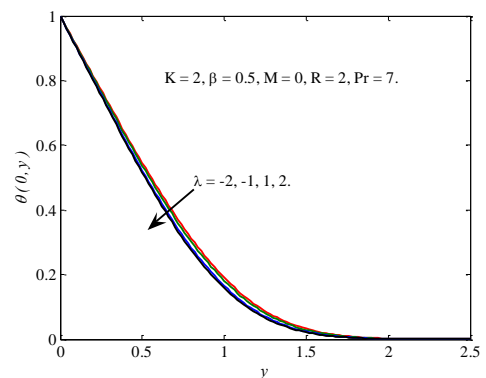


Fig. 18: Effect of the temperature profile for various values of the mixed convection parameter

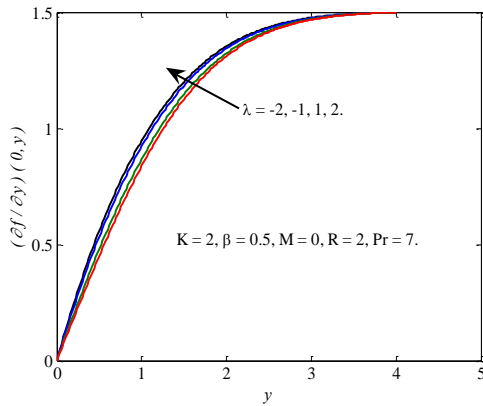


Fig. 19: Effect of velocity field for various values of the mixed convection parameter

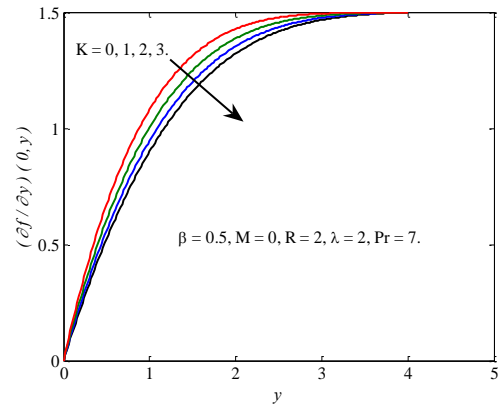


Fig. 22: Effect of velocity field for various values of the micro-rotation parameter

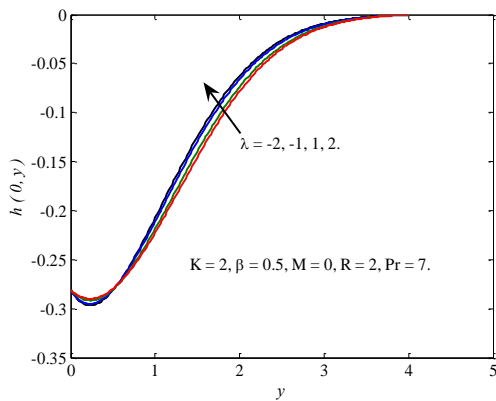


Fig. 20: Effect of angular velocity field for various values of the mixed convection parameter

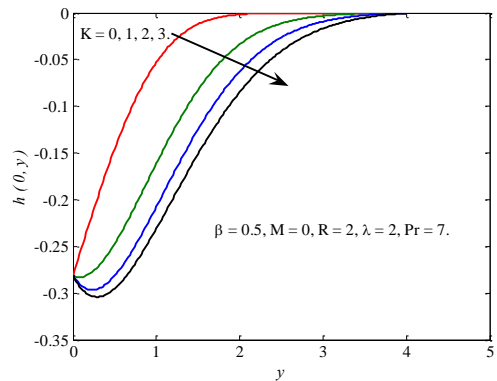


Fig. 23: Effect of the angular velocity profile for various values of the micro-rotation parameter

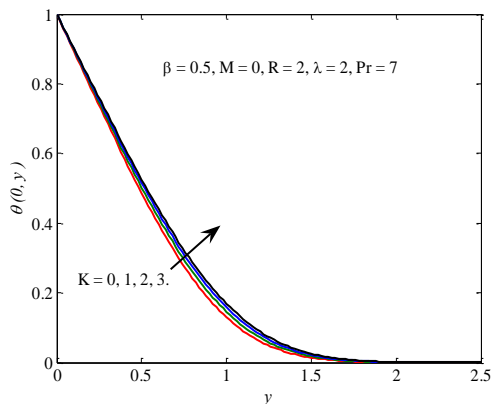


Fig. 21: Effect of the temperature profile for various values of the micro-rotation parameter

CONCLUSION

In this paper, we have studied the problem of mixed convection boundary layer flow over a solid sphere immersed in a micropolar Casson fluid. We investigated the effects of Casson parameter, radiation parameter, mixed convection parameter, magnetic parameter and micro-polar parameter on the flow and heat transfer characteristics. The partial differential equations were solved numerically via the Keller-box method. This study concluded the followings:

- i. An increase in the values of radiation parameter and mixed convection parameter led to an increase in the values of local Nusselt number and local skin friction coefficient. But, the opposite behavior is obtained for the case of the magnetic parameter.
- ii. An increase in the values of Casson parameter led to the increase in the value of local Nusselt number and decreases in local skin friction coefficient. However, an opposite effect is determined for the case of the micro-polar parameter.
- iii. An increase in the values of Casson parameter, radiation parameter, and mixed convection parameter increase will lead to the increment in the velocity and the angular velocity profiles.

Whereas, an opposite influence is determined for the case of the micro-polar parameter.

- iv. The values of temperature profiles increase when the radiation parameter and micro-polar parameter increase. On the other hand, values of temperature profiles decrease when Casson parameter and mixed convection parameter increase.

Nomenclatures

a	Radius of the cylinder;
B	Thermal expansion coefficient;
C_j	Local skin friction coefficient;
c_p	Specific heat;
f	Reduced stream function;
j	Microinertia density;
\bar{H}	Angular velocity of micropolar fluid;
g	Acceleration due to gravity;
Gr	Grashof number;
K	Material or micropolar parameter;
k	Thermal conductivity;
k^*	Mean absorption coefficient;
M	Magnetic parameter;
Nu	Local Nusselt number;
R	Radiation parameter;
Pr	Prandtl number;
p_y	Yield stress of the fluid;
q_w	Constant wall heat flux;
Re	Reynolds number;
T	Fluid temperature;
T_∞	Temperature of the ambient fluids;
u, v	Non-dimensional velocity components along x and y directions;
x, y	Coordinates measured from the lower stagnation point along the surface of sphere and normal to it, respectively;

Greek Symbols

α	Thermal diffusivity;
β	Parameter of the Casson fluid;
λ	mixed convection parameter
ϕ	Spin gradient viscosity;
θ	Non-dimensional temperature;
μ	Dynamic viscosity;
μ_B	Plastic dynamic viscosity of the non-Newtonian fluid;
π_c	Critical value of this product based on the non-Newtonian model;
κ	Vortex viscosity;
σ	Electric conductivity;
σ^*	Stefan-Boltzmann constant;
α	Thermal diffusivity;
ρ	Fluid density;
ν	Kinematic viscosity;
ψ	Non-dimensional stream function.

REFERENCES

1. Ramachandra, P., V;Rao, A.S. and Bég, O.A. (2013). Flow and heat transfer of casson fluid from a horizontal circular cylinder with partial slip in non-darcy porous medium. *Journal of Applied and Computational Mathematics*, 2 (127), 2-12.
2. Casson, N. (1959). A flow equation for pigment-oil suspension of the print ing ink type: Conference of the British society of rheology, Univer sity College, Swansea, UK. *NewYork: Pergamon Press*.
3. Mustafa, M.;Hayat, T.;Pop, I. and Aziz, A. (2011). Unsteady boundary layer flow of a Casson fluid due to an impulsively started moving flat plate. *Heat Transfer Asian Research*, 40 (6), 563-76.
4. Mukhopadhyay, S.;Bhattacharyya, K. and Hayat, T. (2013). Exact solutions for the flow of Casson fluid over a stretching surface with transpiration and heat transfer effects. *Chinese Physics B*, 22 (11), 1-6.
5. Subba, R., A;Ramachandra Prasad, V.;Bhaskar Reddy, N. and Anwar Bég, O. (2015). Heat Transfer in a Casson Rheological Fluid from a Semi-infinite Vertical Plate with Partial Slip. *Heat Transfer Asian Research*, 44 (3), 272-91.
6. Mahdy, A. and Ahmed, S.E. (2017). Unsteady MHD convective flow of Non-Newtonian Casson fluid in

- the stagnation region of an impulsively rotating sphere. *Journal of Aerospace Engineering*, 30 (5), 04017036.
7. Nagendra, N.; Amanulla, C.; Narayana Reddy, M.; Rao, A. and Bég, O. (2017). Mathematical study of Non-Newtonian nanofluid transport phenomena from an isothermal sphere. *Frontiers in Heat and Mass Transfer*, 8, 1-13.
 8. Mehmood, Z.; Mehmood, R. and Iqbal, Z. (2017). Numerical Investigation of micropolar Casson fluid over a stretching sheet with internal heating. *Communications in Theoretical Physics*, 67 (4), 443-48.
 9. Shehzad, S.; Hayat, T.; Qasim, M. and Asghar, S. (2013). Effects of mass transfer on MHD flow of Casson fluid with chemical reaction and suction. *Brazilian Journal of Chemical Engineering*, 30 (1), 187-95.
 10. Khalid, A.; Khan, I.; Khan, A. and Shafie, S. (2015). Unsteady MHD free convection flow of Casson fluid past over an oscillating vertical plate embedded in a porous medium. *Engineering Science and Technology, an International Journal*, 18 (3), 309-17.
 11. Eringen, A.C. (1966). Theory of micropolar fluids. *Journal of Mathematics and Mechanics*, 1-18.
 12. Hassanien, I.; Abdullah, A. and Gorla, R. (1998). Numerical solutions for heat transfer in a micropolar fluid over a stretching sheet. *Applied Mechanics and Engineering*, 3 (3), 377-91.
 13. Papautsky, I.; Brazzle, J.; Ameel, T. and Frazier, A.B. (1999). Laminar fluid behavior in microchannels using micropolar fluid theory. *Sensors and actuators A: Physical*, 73 (1-2), 101-08.
 14. Nazar, R.; Amin, N.; Filip, D. and Pop, I. (2004). Stagnation point flow of a micropolar fluid towards a stretching sheet. *International Journal of Non-Linear Mechanics*, 39 (7), 1227-35.
 15. Sherief, H.; Faltas, M. and Ashmawy, E. (2011). Exact solution for the unsteady flow of a semi-infinite micropolar fluid. *Acta Mechanica Sinica*, 27 (3), 354-59.
 16. Hussanan, A.; Salleh, M.Z.; Khan, I. and Tahar, R.M. (2018). Heat and mass transfer in a micropolar fluid with Newtonian heating: an exact analysis. *Neural Computing and Applications*, 29 (6), 59-67.
 17. Hussanan, A.; Salleh, M.Z.; Khan, I. and Tahar, R.M. (2015). Unsteady free convection flow of a micropolar fluid with Newtonian heating: Closed form solution. *Thermal Science*, (00), 125-25.
 18. Alkawasbeh, H.T.; Salleh, M.Z.; Tahar, R.M.; Nazar, R. and Pop, I. (2014). Free Convection Boundary Layer Flow on a Solid Sphere with Convective Boundary Conditions in a Micropolar Fluid. *World Applied Sciences Journal*, 32 (9), 1942-51.
 19. Alkawasbeh, H. (2018). Numerical solution on heat transfer magnetohydrodynamic flow of micropolar casson fluid over a horizontal circular cylinder with thermal radiation. *Frontiers in Heat and Mass Transfer (FHMT)*, 10.
 20. Swalmeh, M.Z.; Alkawasbeh, H.T.; Hussanan, A. and Mamat, M. (2018). Heat transfer flow of Cu-water and Al₂O₃-water micropolar nanofluids about a solid sphere in the presence of natural convection using Keller-box method. *Results in Physics*, 9, 717-24.
 21. Waqas, H.; Hussain, S.; Sharif, H. and Khalid, S. (2017). MHD forced convective flow of micropolar fluids past a moving boundary surface with prescribed heat flux and radiation. *Br. J. Math. Comput. Sci.*, 21, 1-14.
 22. Yuge, T. (1960). Experiments on heat transfer from spheres including combined natural and forced convection. *Journal of Heat Transfer*, 82 (3), 214-20.
 23. Hieber, C. and Gebhart, B. (1969). Mixed convection from a sphere at small Reynolds and Grashof numbers. *Journal of Fluid Mechanics*, 38 (1), 137-59.
 24. Chen, T. and Mucoglu, A. (1977). Analysis of mixed forced and free convection about a sphere. *International Journal of Heat and Mass Transfer*, 20 (8), 867-75.
 25. Dennis, S. and Walker, J. (1971). Calculation of the steady flow past a sphere at low and moderate Reynolds numbers. *Journal of Fluid Mechanics*, 48 (4), 771-89.
 26. Tham, L.; Nazar, R. and Pop, I. (2011). Mixed convection boundary-layer flow about an isothermal solid sphere in a nanofluid. *Physica Scripta*, 84 (2), 025403.
 27. Alkawasbeh, H.T.; Salleh, M.; Tahar, R.; Nazar, R. and Pop, I. (2015). Numerical Solution for Mixed Convection Boundary Layer Flow About a Solid Sphere in a Micropolar Fluid with Convective Boundary Conditions. *World Applied Sciences Journal*, 33 (9), 1472-81.
 28. Cebeci, T. and Bradshaw, P. (2012). Physical and computational aspects of convective heat transfer. Springer Science & Business Media.
 29. Nazar, R.; Amin, N. and Pop, I. (2002). Free convection boundary layer on an isothermal horizontal circular cylinder in a micropolar fluid. *Heat Transfer*, 2, 525-30.
 30. Bataller, R.C. (2008). Radiation effects in the Blasius flow. *Applied Mathematics and Computation*, 198 (1), 333-38.
 31. Nazar, R.; Amin, N. and Pop, I. (2003). Mixed convection boundary layer flow about an isothermal sphere in a micropolar fluid. *International journal of thermal sciences*, 42 (3), 283-93.